

# Self-aware Data Processing for Power Saving in Resource-Constrained IoT Cyber-Physical Systems

Ehsan Hadizadeh Hafshejani, Nima TaheriNejad, Rozhan Rabbani, Zohreh Azizi, Shahabeddin Mohin, Ali Fotowat-Ahmady, and Shahriar Mirabbasi, *Member, IEEE*

**Abstract**— Given the emergence of the Internet of Things (IoT) Cyber-Physical Systems (CPSs) and their omnipresence, reducing their power consumption is among the major design priorities. To reduce the power consumption of such systems, we propose the use of a signal-dependent sampling method in a bottom-up fashion, which can lead to up to a 94% reduction in the overall system power with negligible or no loss in performance. Moreover, the proposed technique provides further flexibility for self-aware CPSs to dynamically adjust the number of data samples that are needed for processing (and consequently reduce the power consumption) based on the application at hand and the desired trade-off between accuracy and power consumption. To show the merits of the proposed approach, we also present case studies in the context of an Electrocardiography (ECG) monitoring system as well as a greenhouse (temperature and relative humidity) monitoring system. We also discuss the trade-offs among the system configuration parameters, power consumption, and performance (accuracy). We show that the proposed method has a negligible overhead, which facilitates the real-time operation of the IoT CPS while achieving significant power savings (up to 94%). Even though we study the effects of using this method for two representative applications, the technique is general and can offer similar improvements for a wide range of CPSs and resource-constrained IoT systems.

**Index Terms**— Signal-dependent sampling, Non-uniform sampling, Internet of Things, Cyber-physical systems, Embedded systems, Wearable healthcare systems, Electrocardiography (ECG) monitoring, Green-house monitoring.

## I. INTRODUCTION

THE number of devices that are connected to the Internet, in general, and the wearable healthcare devices, in particular, are continuously growing. In recent years, the number of such connected devices have already exceeded the world's population [1]. This number is expected to further grow, and by the end of 2023 it is estimated that Internet of Things (IoT) technology connects more than 25 billion devices [2]. Many of these devices enable important applications such as Wearable Health-care Systems (WHS) which facilitate improved healthcare and well-being for the general public (including athletes, patients, and elderly people) at the comfort of their personal and/or professional work environments. Another example application is environmental monitoring, for instance, temperature and humidity monitoring of houses and green houses, which would result in energy savings, improved quality of life and/or cost-efficient crops production [3]–[5]. While the number of sensors and processing elements keeps growing on many IoT and wearable devices, the power budget available to them (in particular in WHS) is usually limited and does not grow at the same rate [6]–[8]. This leads to an increasing gap between the available power and required power for such devices to properly function. Therefore, power management and reducing power consumption is one of the top priorities.

In wearable devices and Cyber-Physical System (CPS) at the edge of IoT, the power required for sampling the outputs

of sensors, storing the sampled data, and processing it is typically a sizable portion of the overall power consumption. Having more sensors not only results in increased power consumption for more data collection, but also causes further increase in power consumption of other blocks of the system. For example, when in addition to data storage some data processing and analysis is performed on the Embedded System (ES) itself, or power is consumed to communicate data when the data needs to be transmitted to an external unit in the fog or cloud layer [9]–[12]. Therefore, techniques that can reduce the number of samples that are required to represent the original sensory data with no to minimum compromise on the quality of the signal are highly desirable [13], [14]. Many such techniques such as compressed sensing [15]–[17], Digital Compression (DC) [18]–[20], and nonuniform sampling methods [21] including event-based sampling techniques [22] and signal-dependent sampling [23] have been used to alleviate the cost of conventional Nyquist-rate (uniform) sampling.

Previously, we have shown how an analog signal-dependent sampling circuit can be implemented and integrated into sampling circuit (before Analog-to-Digital Converter (ADC)) [23]. However, changing the internal Application Specific Integrated Circuit (ASIC) design of an ES is not always a cost-effective solution. Furthermore, in many applications, to improve the time-to-market, it is desired to implement IoT devices using off-the-shelf components. Therefore, in this work, we propose and show how we can use the concept of signal-dependent sampling at the system-level to save power. Furthermore,

we show that by changing only the underlying software in an existing ESs one can achieve performance improvements (especially, regarding power-consumption) in resource-constrained systems. As proof-of-concepts, we evaluate this technique in the context of an ECG-based WHS and IoT-edge device for monitoring and controlling the temperature and relative humidity of green houses in a self-aware fashion. Since different applications require different levels of accuracy, it is important to be able to tune/control the number of required samples to reproduce the signal with the desired quality. Such tunability is offered by the proposed approach, which allows the system to reduce its power consumption while still meeting the accuracy requirements. We investigate various parameter settings and present their effects on the performance (accuracy of detection) and power savings of the system for different applications.

The organization of the rest of the paper is as follows: Section II overviews the concepts of top-down and bottom-up design in self-aware systems. Section III analyzes the power consumption in IoT ES and CPS, and provides insights in identifying changes in the system that are most effective in reducing power. Section IV presents the signal-dependent sampling technique in the context of the proposed CPSs. Section V shows the hardware setup and test bench of our proof-of-concept ECG system. Section V-C presents the performance of the proposed method in a variety of end-applications based on ECG. Section VI showcases using the proposed method in an IoT system for monitoring the temperature and relative humidity of a green-house. In Section VII, we summarize the performance improvements as well as the overhead due to the use of the proposed method. In Section VIII, we compare the proposed method with other state-of-the-art works in the literature. Section IX provides concluding remarks.

## II. A BRIEF OVERVIEW OF COMPUTATIONAL SELF-AWARENESS

One of the techniques, which has been proven to be helpful in reducing the amount of data and data processing is computational self-awareness, see e.g., [13], [24]–[27]. Computational self-awareness has been studied and applied in a wide range of cyber-physical applications [28], such as machine learning [29]–[32], industrial applications [33], [34], and healthcare systems [13], [30], [35]. In such a self-aware system, the system monitors itself and its performance, and adjusts its operation based on the internal and external conditions to meet the desired requirements [36]. Such decisions (e.g., adjusting the number of data samples) could be taken in a top-down or a bottom-up fashion [37].

In the top-down decision making, at the high-level and based on the overall system goals and conditions, the decisions to adjust the operation of the sensory unit are made [38]. For example, in [13], based on the health conditions of the subject and its current activities, the system adjusts the sampling rate and communication settings of the sensors and the wearable gadget to save up to 50% in power consumption. Although the power saving is significant, such top-down approaches can be conservative [24], [39] and thus there may be further room for performance improvements.

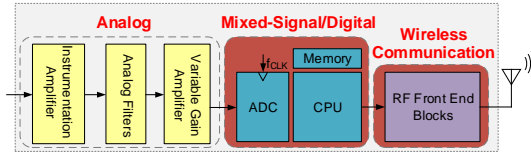


**Fig. 1:** Block diagram of a typical wireless-connected IoT gadget.

Another approach is the bottom-up decision making, where some decisions are initiated and made at the lower levels of the system. For example, the sensory module itself can change its sampling rate based on the changes that it observes in the incoming signal [14], [26]. In such approaches, a critical concept is the definition of “events” or “changes” which heavily depends on the application. An optimal setting for one application could be either too conservative or too inaccurate for another application which could lead to unnecessarily large power consumption or loss of information. To avoid such undesired conditions, the designer during the design process (design-time) or the (self-aware) system during the run-time should be able to tune/adjust the parameters of the system to ensure an optimal operation. This property is one of the key features of the proposed method and we will show how the proposed approach improves on the properties of the IoT systems, especially power consumption, without compromising the functionality of the system.

## III. POWER CONSUMPTION IN IoT SYSTEMS

To find a solution for reducing the power consumption of IoT devices, it is important to understand the contribution of various building blocks of the system to the overall power consumption. Generally, as shown in Figure 1, an IoT system consists of the following subsystems; an analog block (sensors and their associated interface circuits), a mixed-signal/digital block (ADC and digital signal processing and storage blocks such as a micro-controller and a memory unit), and the (wireless) communication block. Contribution of each block to the power consumption depends on many factors including the technology used, the application, and the communication protocol. Here, as a representative example, we further analyze the power consumption of different building blocks of a typical ECG patch with Bluetooth Low Energy (BLE) connection.

### A. The Analog Block

For an ECG patch, the analog block includes an Instrumentation Amplifier (IA) to amplify the signal to a reasonable level, analog filters to reject the out-of-band noise, and a Variable Gain Amplifier (VGA) to control the overall gain of the analog front-end. Without loss of generality and for the simplicity, we assume that off-the-shelf components are used for implementation of all of these blocks. In the example of the prototype system that we have implemented, the total power consumption of the analog block is  $P_{AFE} = 8\mu A \times 3V = 24\mu W$ . Considering that in a real-time monitoring system, the analog block must be continuously operating, the overall power consumption of the system is more than  $P_{AFE}$ .

### B. Mixed-Signal and Digital Blocks

These blocks of the system typically consist of three main sub-blocks: the data conversion unit such as an ADC, the processing unit such as a processor, and the data storage unit, such as a memory. For example, in one of our prototype implementations (ECG monitoring system), the processor is an ARM Cortex-M3 and all the three sub-blocks, namely, the ADC, the processor and the memory unit are included in a TI-CC2650 System-on-Chip (SoC). The current draw of the overall mixed-signal and digital blocks is around 2.3 mA when the system is operating in its active mode and less than 1  $\mu$ A when it is in its standby mode [40]. In this applications, since the data transfer rate of the wireless block of the system, which is based on the (BLE) protocol, is 1 Mb/s [41], and is much higher than the standard sampling rate of ECG (i.e., < 1 kS/s), the microcontroller can collect the ECG samples for specific time intervals and then transmit the collected data at the end of each such interval. This approach could help the microcontroller and Radio Frequency (RF) front-end circuits to be in standby mode (sleep mode) during the most of the time interval that the data is being collected. As a result, the power consumption can be lowered. For the process of sampling, the microcontroller is in standby mode for most of the time and only at each sampling clock edge wakes up and samples and stores the taken sample. The power consumption of the microcontroller (which includes the ADC, processor, and memory units) can be written as follows:

$$P_{MCU} = (f_s \times t_{MCU} \times I_{MCU}) \times V_{DD} \quad (1)$$

where  $f_s$  is the sampling frequency required for the application (for example, for ECG), and  $t_{MCU}$  is the time that the microcontroller needs to be active in order to take and save a sample from the input signal.  $V_{DD}$  and  $I_{MCU}$  are the supply voltage of the microcontroller and the current drawn from the supply when microcontroller is in its active mode. Based on the measurements, the overall energy consumption for "one" sample to be taken and stored is  $224 \mu\text{s.mA} \times V_{DD}$ . Considering  $V_{DD} = 3 \text{ V}$ , (1) can be written as:

$$P_{MCU} = (f_s \times 0.224 \times 3) \mu\text{W}. \quad (2)$$

Due to using BLE, when the number of collected samples reaches a predefined value, the microcontroller will turn on the RF front-end circuits to send out the collected samples to the external receiver device.

In this paper, using a bottom-up approach in the form of signal-dependent sampling, we substantially reduce the number of samples to be transmitted and thus reduce the number of times that RF front-end needs to be turned on. Thus, we significantly reduce the overall power consumption of the system, without changing underlying hardware of the system. We will show that the processing overhead for such a power saving is negligible.

### C. Wireless Communication Block

The wireless communication block or RF block of the system is based on a BLE system, which is a Bluetooth protocol that is designed for low-power systems [42]. This protocol is

designed to facilitate the possibility of the peripheral device (here the ECG patch) to go into the sleep mode [43].

The used TI-CC2650 SoC includes an RF core which supports BLE protocol. The current draw of this RF core in its transmit mode (receive mode) is 9.1 mA (6.5 mA). Note that each time that the RF block is turned on (coming out of sleep mode), there is a setup time needed and the energy consumption of the circuit during these setup times needs to be taken into account [44] [45]. We can model the energy consumption with

$$E_C = E_{setup} + E_{Tx} + E_{Rx} + E_{Tx/Rx} \quad (3)$$

where  $E_C$  is the total energy per connection,  $E_{setup}$  is the energy consumption during RF front-end setup,  $E_{Tx}$  and  $E_{Rx}$  are energy consumption of transmitting data and receiving acknowledgments needed for the BLE protocol, and  $E_{Tx-Rx}$  is the energy needed to change from transmit mode to receive mode and vice versa. The two plots in Figure 2 show the details of different actions and energy consumption of a Connection Event (CE). Figure 2a depicts current drawn from the supply and the duration of different actions of a CE, in which 100 bytes of data are sent. For sending 100 bytes, the transmitter has to send 5 sequential packets in a CE. Figure 2b shows the measured energy consumption (current  $\times$  time  $\times$   $V_{DD}$ ) of each part during a connection event in which 100 bytes of data are sent from ECG patch to the external device (in this case, a smartphone). If we split the data into 100-byte packets, and given that each data sample is one byte, using Equation (3) we can calculate the total power consumption of the RF core as:

$$\begin{aligned} P_{RF} &= \frac{f_s}{100} \times E_C \\ &= \frac{f_s}{100} \times (7.4 + 23.5 + 6.5 + 6.9)_{\text{ms.mA}} \times V_{DD} \\ &= (f_s \times 0.443 \times 3) \mu\text{W} \end{aligned} \quad (4)$$

Thus, the total power consumption of the patch can be calculated as follows:

$$\begin{aligned} P_{tot} &= P_{AFE} + P_{MCU} + P_{RF} \\ &= (8 + 224 + 443) \mu\text{A} \times 3 \text{ V} \\ &= 2025 \mu\text{W} \end{aligned} \quad (5)$$

### D. Power Consumption and Sampling Rate

Figure 3 shows the contribution of each block to the total power consumption. As it can be seen in Equation (2) and Section III-C, the power consumption of the system is directly proportional to the sampling rate of the input signal. Therefore, considering Figure 3, we observe that more than 98% of the power consumption is proportional to the sampling rate. This motivates the work of this paper, where we use a Signal Dependent Sampling (SDS) technique to reduce the number of samples to be transmitted which results in power saving.

## IV. PROPOSED APPROACH

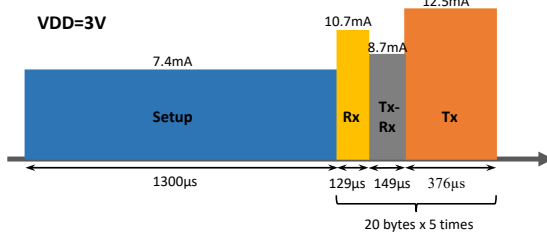
As shown in Section III, the sampling frequency plays a crucial role in the overall power consumption of an IoT device.

Reducing the frequency of sampling in a top-down fashion may lead to loss of valuable information, therefore, in the top-down approach the chosen sampling rate may be conservative. On the other hand, most bottom-up approaches [46], [47], [48], and [23], are implemented at the circuit level. Changing the circuit level structure of an IoT device may not be the most cost-effective solution and/or would require a longer time-to-market. Hence, in contrast to [23], here, we propose using a software-based approach to reduce the power consumption in a bottom-up fashion using a SDS technique. In this section, we briefly explain the principles of the SDS technique used here that decreases the overall number of samples to be processed. As it will be shown, the proposed method can lower the average power consumption (for example, by up to 90% in an ECG patch, and by up to 94% in a green-house monitoring system), *without requiring any hardware changes*. In addition, the approach is compatible with self-aware computing, in that it allows the system to dynamically adjust the accuracy (and consequently the power consumption) of the system based on the requirements and available resources. The signal-dependent sampling technique used here approximates the signal with its piece-wise linear representation (i.e., with a

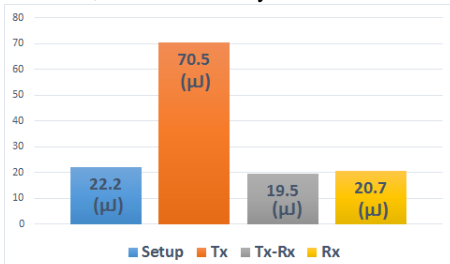
sequence of connected linear segments). The decision on which samples (end points of each line segment) to keep is made in a bottom-up fashion at the lower level of the system by the sensory module. The sensory module makes this decision based on the approximation of the second derivative of the signal waveform, which is an indication of the rate of change of the signal. In other words, because we want to approximate the signal with pieces of lines, as long as a group of samples can be fitted to a line, we can keep the start-point and the end-point samples and the time difference between those points. To check that the new sample is approximately along the same line as the others, we can compare the slope of the current line with the slope of the line that the new sample makes with the current end-point. If these two slopes are close, it means the new sample is approximately on the same line. Thus, we can put the new sample as the new end-point of the line and eliminate the previous end-point. To implement this algorithm and decide whether a sample should be retained (making a new line segment) and later sent to the external gateway device via RF front-end, the following equation is used:

$$\left| \frac{x[n-1] - x[n-m-1]}{(m+1) \times T_s} - \frac{x[n] - x[n-1]}{T_s} \right| \leq \varepsilon, \quad (6)$$

where  $x[i]$  is the  $i$ -th sample,  $n$  is the index of the current sample,  $m$  is the number of discarded samples,  $T_s$  is the sampling period, and  $\varepsilon$  is a variable that determines the acceptable error between the slope of the original line segment and the estimated slope. Figure 4 shows the block diagram for implementing this process.



(a) Current draw and the duration of different actions of a connection event, in which 100 bytes of data are sent.



(b) Energy consumption of different actions of a connection event, in which 100 bytes of data are sent.

**Fig. 2:** Energy consumption of a connection event.

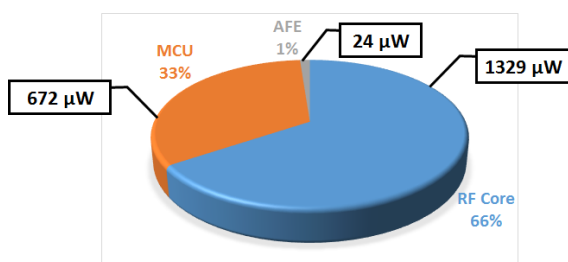


**Fig. 3:** Contribution of system blocks to the total power consumption

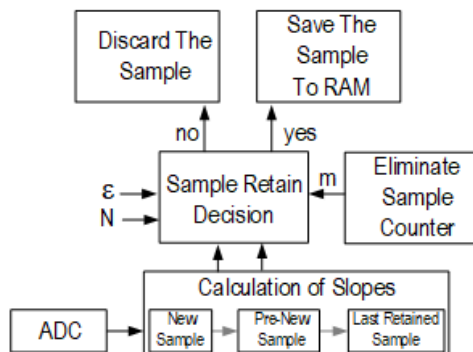


**Fig. 4:** Block diagram of the proposed method of using SDS for maintaining or discarding samples.

The first term on the left-hand side of the inequality represents the relative slope of the line segment between  $x[n-1]$  and  $x[n-m-1]$  and the second term indicates the slope between  $x[n]$  and  $x[n-1]$ . If the two slopes are close (their difference is  $\leq \varepsilon$ ),  $x[n-1]$  can be discarded. Otherwise, the sample is retained. The example in Figure 5, shows the dependence of the number of retained samples (yellow dots) to the shape of the signal and the reconstructed signal for the traditional Nyquist sampling (red dots, gray line) compared to the SDS (yellow dots, blue line).

It can be shown that the worst-case error due to SDS

sampling is:

$$|e[i]| = |x[i] - \hat{x}[i]| = \left( \sum_{j=i+1}^N \left( \frac{1}{j} \right) \right) \times \varepsilon \times i \times T_s \quad (7)$$

where  $x[i]$  represents the signal sample at time index  $i$ ,  $\hat{x}[i]$  is the reconstructed output of the SDS,  $N$  is the maximum number of discarded samples, and  $e[i]$  is the difference between the original samples and the reconstructed samples, which can be modeled as an added error to the reconstructed signal. In this method, the error can be either controlled by  $\varepsilon$  or  $N$ . By setting lower values for  $\varepsilon$ , the error can be reduced at the cost of higher number of retained samples. The second approach is to control the error by  $N$ . By limiting the maximum number of discarded samples one can also control the error. Thus, by proper selection of  $\varepsilon$  and  $N$ , one can trade-off between the added error and the number of discarded samples.

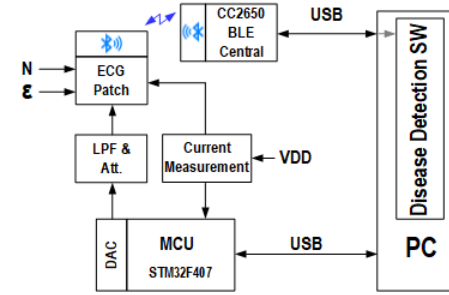
To demonstrate the advantages of the proposed method, we have applied it to two IoT wireless sensor systems, namely an ECG patch and a green-house monitoring system and the results are presented in the following sections.

## V. ECG PATCH

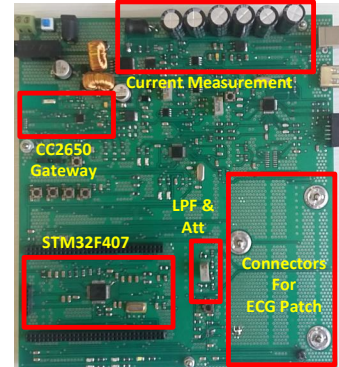
### A. Evaluation Test-Bench

To evaluate the performance of the system, we need a test-bench, which could provide ECG signal to the input of the ECG patch, measure the power consumption of the patch, and retrieve the output of the patch via BLE to analyze the output data. For this purpose, we have designed a test-bench whose block diagram is shown in Figure 6a and its implementation on a Printed Circuit Board (PCB) is shown in Section V-A. The test-bench consists of the following blocks: A STM32F407 ARM microcontroller [49], which is connected to a Personal Computer (PC) to send and receive commands and data. The microcontroller also emulates and provides the appropriate ECG signal to the ECG monitoring system using a 12-bit Digital to Analog Converters (DACs). The prepared emulated ECG signal is filtered and attenuated to mimic a real ECG signal level ( $< 1 mV_{pp}$ ) and is fed to the ECG patch. Note that to have a realistic set of input data, these ECG signals are chosen from the database of the “Laboratory for Computational Physiology” of Massachusetts Institute of Technology (MIT), “Physiobank” [50]. The microcontroller also measures the

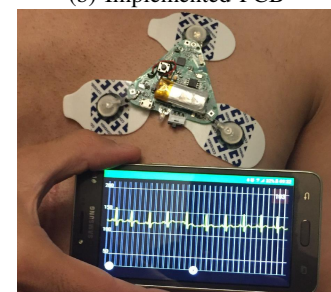
current draw of the ECG patch using a current measurement circuit to enable us to calculate the power consumption of the patch. The current measurement circuit includes a low-pass filter and a current-to-voltage converter circuit. The settling time of the low-pass filter is designed to be very large ( $> 1$  s) to also take into account the average supply current during the current spikes when turning on and off the ECG patch to have a fairly accurate measurement of the average power. The current-to-voltage converter circuit [51], with a proper gain, converts the average current to a voltage which can be sampled using the ADC of the microcontroller. The next sub-block of the test-bench is a BLE SoC (TI-CC2650), which plays the role of the “gateway” device (in a typical field operation a smartphone could be used instead) to receive sampled ECG data from the patch and send the received data to the PC for software analysis. Note that as mentioned earlier, the ECG patch includes its own microcontroller unit (CC2650 from TI) which provides ADC as well as processing and storage units, and the BLE RF unit).



(a) Schematic block diagram



(b) Implemented PCB



(c) Sensor and Mobile App.

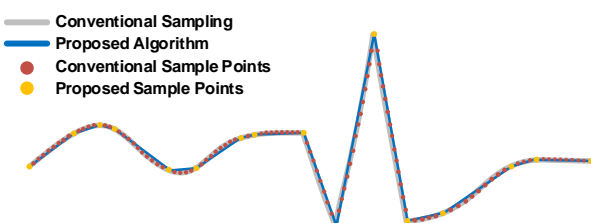


**Fig. 5:** Example signals to visualize the SDS method. Red dots show the traditional sampling points and the yellow dots show the samples retained by this method. The gray signal is the reconstructed signal based on the traditional sampling while the blue one is reconstructed based on the SDS approach.

**Fig. 6:** Evaluation test bench.

### B. Fidelity of the Sampled ECG Signal

To study the effect of the presented sampling technique we inject various ECG signals from “Physiobank” database [50] to the test bench and evaluate the performance of the implemented system. For each imported ECG record, we use different values of  $N$  and  $\epsilon$  for sampling the signal using the described SDS. The power consumption of the patch and the sampled data for each record are analyzed using MathWorks®MATLAB to study the effect of the presented technique on the average number of samples as well as the accuracy of reconstructed ECG signal. Figure 7 shows an ECG signal, which is sampled using both the conventional Nyquist-rate sampler and the presented SDS. The blue lines show the reconstructed Nyquist-rate sampled signal and the red lines show the reconstructed signal using SDS with four different configurations.

In these tests,  $(\epsilon, N)$  is set to  $(60\text{mV}, 20)$ ,  $(60\text{mV}, 40)$ ,  $(70\text{mV}, 75)$ , and  $(55\text{mV}, 256)$ . The results in Figure 7 show that as  $N$  increases, the Compression Factor (CF) –the ratio of Nyquist rate sampling rate to SDS average sampling rate– increases, at the cost of some deteriorations in the details of the signal. In the case of  $N=256$ , even though the Post-Reconstruction Signal-to-Noise plus Distortion Ratio (PR SNDR) is very low ( $4.9 \text{ dB}$ ), many meaningful information can still be extracted from the signal. However, to better detect health disorders for which the details are important, lower values of  $N$  and  $\epsilon$  can be used. On the other hand, to detect health issues for which only heart beats and a coarse estimate of ECG are required, we can use a higher value for  $N$  and  $\epsilon$ , which results in a higher CF and offers a higher saving in power. We discuss this in further details in Section V-C.

### C. ECG Patch Case Study

In general, the amounts of data compression and power savings are in trade-off with the acceptable error in the reconstructed signal. The amount of the acceptable error in the reconstructed data is dependent on the end-use application. Here, we will study the effect of the presented SDS on the detection of some common ventricular problems. To this end, we first take a closer look at the ECG signal and its features.

### D. ECG Signal Basics

The ECG signal is described by its different waves, segments, and intervals. Each wave represents a specific activity of the heart. These waves and the intervals between them provide many useful information including atrial and ventricular depolarisation and repolarisation, heart rate, rhythm, blood flow to the heart muscle, effect of abnormal blood pressure, previous heart attacks, to name a few [52]. Figure 7 shows some of the important waves in the ECG signal. The waves are labeled using the letters P, R, and T. P-wave corresponds to the depolarisation of the atrial myocardium (muscles of the upper chambers of the heart), and indicates the start of the atrial contraction that pumps blood to the ventricles [52]. The R-wave (or R-peak) reflects the depolarization of ventricular myocardium, and indicates the start of the ventricular contraction that pumps blood to the lungs and the rest of the

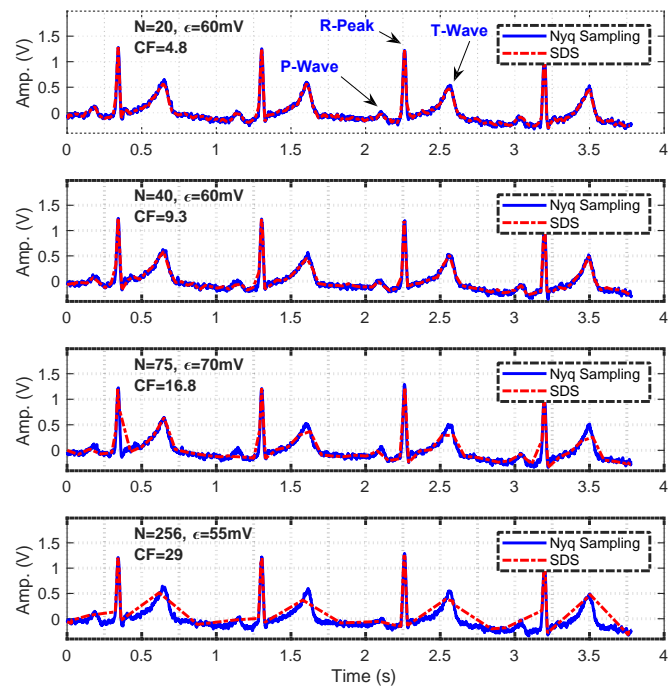


**Fig. 7:** Sampled ECG signal using Nyquist rate (reference) and SDS for three configurations and their effect on the quality of the signal.

body. The T-wave corresponds to the repolarisation of the ventricular myocardium, which is a necessary recovery process for the myocardium to depolarise and contract again [52]. The waves and intervals between them provide useful information to physicians.

### E. Cardiovascular Application Analysis

We have developed a custom C# software based on the algorithms in [53] for analysis of ECG signal and here we study the effects of the proposed sampling technique using the developed software. As mentioned earlier, to provide ECG data that includes disease and arrhythmia, we have used the “Physiobank” database [50]. This database provides an extensive amount of recorded ECG data from healthy subjects and patients who have various cardiovascular diseases. We fed several ECG signals to the sensor, which we sampled using the presented SDS and provided the reconstructed signal to a disease detection software to further study the effects of various values of  $N$  and  $\epsilon$  on the accuracy of the disease detection and also compare the performance of the proposed system with that of the traditional Nyquist-based system. In these tests,  $\epsilon \times T_S$  is swept from 1 to 7 with a step-size of 1, and  $N$  is swept from 10 to 200 with a step-size of 10.

### F. Accuracy of End-Application Analyses

Here, we briefly overview some parameters and cardiovascular disorders and then discuss the results of their analysis using the software. Based on the required accuracy for each application, one can select proper values for sampling parameters to achieve the optimum power saving in the ECG monitoring

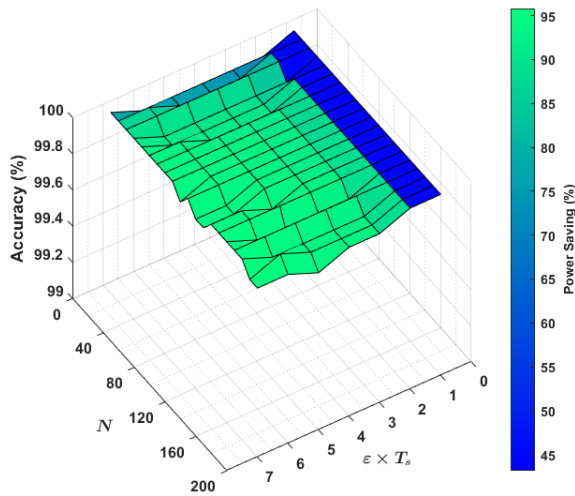


**Fig. 8:** Accuracy of heart rate calculation and bradycardia arrhythmia detection vs power consumption of the patch for various sampling parameter configurations.

system. In the rest of this paper, percentage of power saving ( $P_S(\%)$ ) is defined as

$$P_S(\%) = \left(1 - \frac{P_{SDS}}{P_{Nyq}}\right) \times 100, \quad (8)$$

where  $P_{SDS}$  is the power consumption of the system that uses the proposed method, and  $P_{Nyq}$  is the power consumption of the system that uses the conventional Nyquist sampling method.

**1) Heart Rate:** The heart rate (i.e., number of heart beats in a minute) can be calculated using the ECG signal by counting the number of the R-Peaks in a given period of time. The accuracy of the heart rate calculation for various sampling parameters is shown in Figure 8. As it can be seen from the figure, the accuracy is more than 99.9% for all cases. Figure 8 also shows the power consumption of the ECG patch in each case as a percentage of power consumption of reference operation mode (conventional patch with Nyquist-rate sampling). The resulted normalized power consumption is between 8% and 55% and for most configurations it is closer to 8%. This means that using SDS we can achieve a power saving up to more than 90% with a little to no compromise on the accuracy of heart rate calculation.

**2) Bradycardia:** This is a condition where the normal heart rate is below a threshold (usually 60 Beat Per Minute (BPM) for an adult) [54]. Since this problem is related to the number of heart beats, it can be identified with a high level of accuracy in all sampling configurations. Figure 8 confirms this statement by depicting an accuracy of more than 99.9% for detection for all cases with the power saving of more than 90%.

**3) Sinus Arrhythmia:** In Sinus arrhythmia, the variation in the R-R intervals (interval between two consecutive R-peaks) is greater than 160 milliseconds. For each ten successive beats, we calculate the difference between the maximum and minimum of each consecutive R to R interval. If the result is more than 160 ms a sinus arrhythmia is detected. As Figure 9 shows using the presented SDS technique, the accuracy of

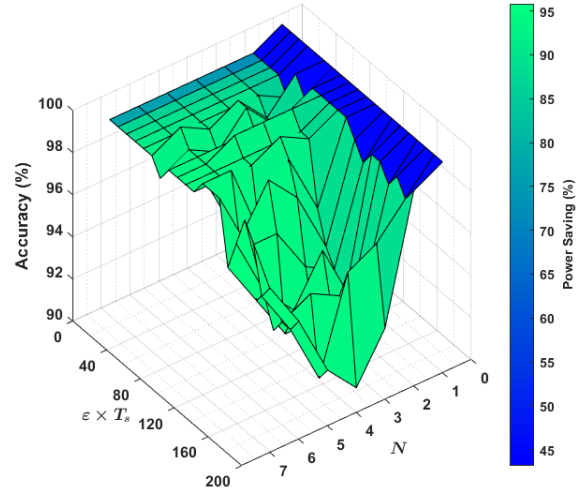


**Fig. 9:** Accuracy of detection of Sinus arrhythmia and power consumption of the patch for various sampling parameters

detection of the sinus arrhythmia is also high (more than 90%), however, it is lower than that of heart rate or bradycardia. Due to the fact that the sinus arrhythmia is detected from the (relative) position of R-peaks, for higher values of  $N$  and  $\varepsilon$ , inaccuracy in the position of R-peaks can cause an error in detection of this type of arrhythmia. As Figure 9 shows, the performance is more sensitive to  $N$  as compared to the  $\varepsilon \times T_s$ , therefore, it seems reasonable to select an  $N$  in the lower range (e.g., around 40), and a medium to large  $\varepsilon \times T_s$  to ensure a high accuracy, while significantly improving the power consumption (by about 90%).

**4) T-wave:** In addition to R-peaks, there are other important waves in the ECG signal. One of these waves is the T-wave. The T-waves are essential to diagnose health issues such as Paroxysmal Atrial Tachycardia (PAT), atrial flutter, and ventricular premature beats (VPBs) [55]–[57]. Thus, here, we study the accuracy of the T-wave detection using the presented approach. Figure 10 shows the accuracy of T-wave detection, which is the ratio of the number of detected T-waves in the presented SDS-based system to that of the reference system (using the conventional Nyquist sampling with no SDS). It shows that for higher values of  $N$  and  $\varepsilon$  the T-waves can be missed, which can also be seen in Figure 7 where for high compression ratios the quality of reconstructed T-waves is deteriorated. Therefore, for applications that require observation of T-waves, conservative values (low  $N$  or  $\varepsilon \times T_s$ ) should be selected. Note that with low  $N$  and high  $\varepsilon \times T_s$  we can achieve lower power consumption as compared to cases with low  $\varepsilon \times T_s$  and high  $N$ . In this case, for an accuracy of more than 97%, up to 78% of power saving for the overall system can be achieved (Figure 10).

## VI. GREEN-HOUSE MONITORING SYSTEM

In this section, we will present another example of IoT CPSs that benefits from the proposed approach. In this implementation, the SDS technique is added to the software of a monitoring system, which tracks and controls the environmental parameters (in this example, temperature and humidity) of a green-house. As shown in Figure 11 the sensor node includes

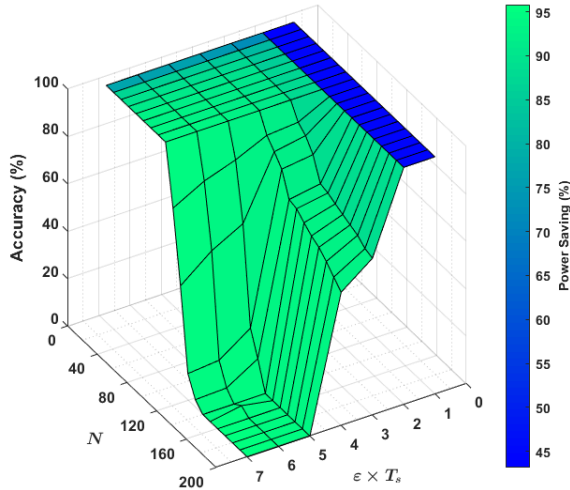


**Fig. 10:** Accuracy of detection of T-Wave and power consumption of the patch for various sampling parameters

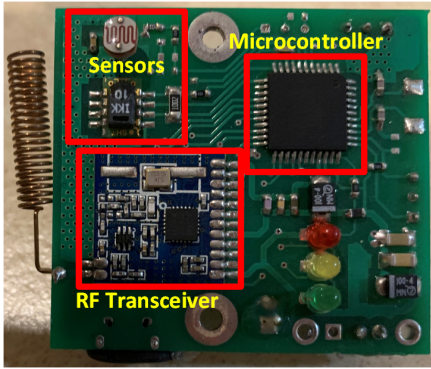


**Fig. 11:** PCB of the wireless sensor node designed for environmental data collection

sensors, a microcontroller, and an RF transceiver. In the normal operation mode, all blocks are in their sleep mode. Every 10 s the microcontroller wakes up and gets a new sample from each of the sensors and send them to the external (e.g., edge) gateway using the RF transceiver. In the proposed system, the procedure is the same. That is, all blocks are in the sleep mode and every 10 s the microcontroller wakes up and gets a new sample from each sensor. However, it does not automatically transmit the samples and rather uses the SDS method to see if the data should be retained or discarded. If the sample should be retained, the microcontroller will turn the RF transceiver on and sends the data to the edge gateway. The gateway processes this data and use it to control the temperature and humidity of the green-house. The gateway system uses the slope and the value of the previous sample that are measured in the SDS approach, to reconstruct the intermediate samples between the previous sample and the new sample. Figure 12 and Figure 13 show the collected temperature and relative humidity (RH) using the proposed approach and the reference approach (Nyquist sampling), respectively. As it can be seen from the figures, the reconstructed signal using the presented approach is fairly close to that of the reference approach. With lower  $N$ s and  $\epsilon$ s, as expected, the reconstruction error would be lower. From the lower sub-graphs of these figures, we can see that by increasing the value of  $N$  and  $\epsilon$ , which in turn

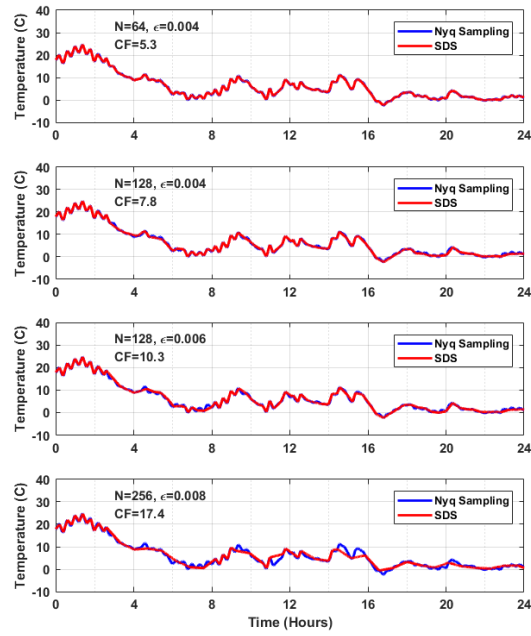


**Fig. 12:** The Result of various  $N$  and  $\epsilon$  setting for temperature measurement and control system

results in a higher CF, the deviation of reconstructed signal based on SDS from the reference signal becomes more visible.

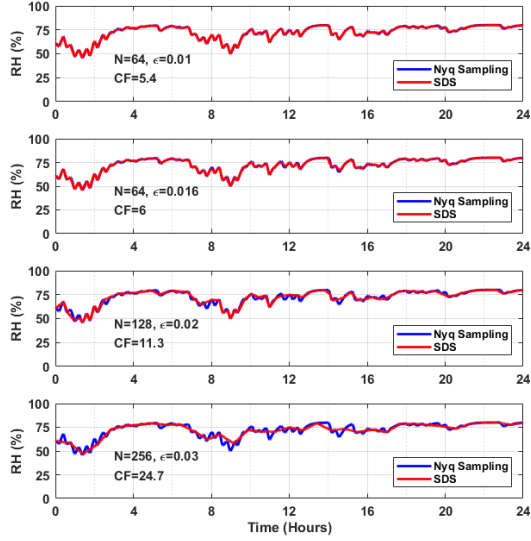
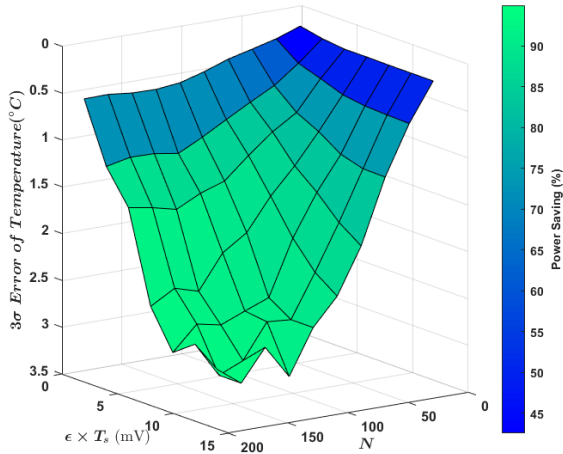
We further studied this effect by sweeping the  $N$  and  $\epsilon$  values and measuring the difference between the temperature and the relative humidity when the systems uses the proposed SDS technique as compared to the reference Nyquist approach. The power consumption of the SDS-based system relative to that of the reference Nyquist-based system is also calculated. Figure 14 and Figure 15 show the results of these experiments for temperature and humidity. As can be seen from these figures, the  $3\sigma$  of temperature difference (and percentage humidity difference) between the two methods is less than  $3^\circ$  (and 6%), whereas the saving in the power consumption is at least 45% and can go up to 94%. In these figures,  $\sigma$  is standard deviation of the difference between the corresponding parameter (temperature or relative humidity) in Nyquist mode and SDS mode. From Figure 14 and Figure 15, we observe that lower to mid values of  $N$  are more suitable, i.e., they result in higher power savings with very little to no loss in the accuracy. Regarding the  $\epsilon$ , or more importantly,  $\epsilon \times T_S$ , however, the suitable range for temperature and humidity differ from each other. For the temperature, as also summarized in Table II, the lower values of  $\epsilon \times T_S$  (that is,  $2 \leq \epsilon \times T_S \leq 8$ ) are more suitable. For the humidity, on the other hand, middle to lower-mid values (that is,  $10 \leq \epsilon \times T_S \leq 40$ ) are more beneficial. The suitable range for  $\epsilon \times T_S$  depends on the slope of the variations of the signal, and the larger the slope of variations the larger the value should be. Thus, given that the slope of variations in humidity is higher than that of the temperature, higher values of  $\epsilon \times T_S$  are more suitable for humidity.

## VII. SELF-AWARE MONITORING USING SDS

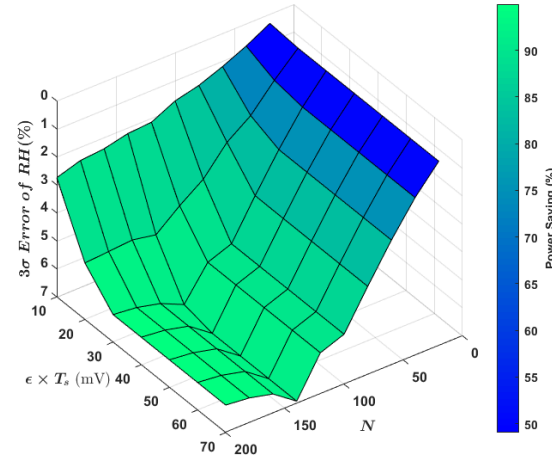
Table II presents a performance summary of the proposed method for various applications of ECG and environmental monitoring. While the proposed SDS method decides which

**TABLE I:** Performance summary of SDS in an ECG patch and green-house monitoring system.

End-application	Accuracy range	Power improvement	Recommended N	Recommended $\varepsilon \times T_S$
Heart rate	100 down to 99.9%	45 to 90%	$80 \leq N \leq 160$	$3 \leq \varepsilon \times T_S \leq 7$
Bradycardia	100 down to 99.9%	45 to 90%	$80 \leq N \leq 160$	$3 \leq \varepsilon \times T_S \leq 7$
Sinus	100 down to 90%	45 to 90%	$40 \leq N \leq 120$	$3 \leq \varepsilon \times T_S \leq 7$
T-Wave	100 down to 97%	45 to 78%	$20 \leq N \leq 80$	$2 \leq \varepsilon \times T_S \leq 4$
Temperature	0.1 to 3 °C(3σ)	45 to 94%	$40 \leq N \leq 150$	$2 \leq \varepsilon \times T_S \leq 8$
Relative Humidity	0.3 to 6 % (3σ)	45 to 94%	$40 \leq N \leq 150$	$10 \leq \varepsilon \times T_S \leq 40$

**Fig. 13:** The Result of various N and  $\varepsilon$  setting for relative humidity measurement and control system**Fig. 14:** 3σ of temperature difference between SDS and reference Nyquist approach and the power consumption of the wireless sensor using the proposed SDS technique relative to that of the reference Nyquist approach for various sampling parameters

data points should be sent for processing, the results summarized in this table (or similar ones for other applications) can be used in a self-aware resource-constrained IoT ES to set the abstraction and accuracy level at run-time and in a top-down fashion. To do so, the self-aware system can tune  $N$  and  $\varepsilon \times T_S$  based on the application and the monitored parameters (for example, based on the type of disease or the

**Fig. 15:** 3σ of the difference between relative humidity of the proposed SDS and reference Nyquist approach and the power consumption of the wireless sensor using the proposed SDS technique relative to that of the reference Nyquist approach for various sampling parameters.

environmental parameter for the applications presented in this paper) and available resources. In our example, the memory overhead of using the proposed method is less than 1 kB of flash memory, and less than 20 B of RAM (for systems with 16 bits or lower-resolution ADCs). The processing time overhead is less than 2  $\mu$ s, which is negligible for this and many other applications, allowing the system to remain real-time. For instance, the standard (Nyquist) sampling rate of ECG is < 1 kS/s, leading to 1 ms time gap between each two samples. Hence, the less than 2  $\mu$ s processing overhead is more than two orders of magnitude smaller than the allowed range for remaining real-time. For the green-house monitoring system the desired sampling rate is much lower (0.1 S/s), making the processing overhead time further insignificant. Given the compactness and simplicity of the proposed approach, it can be implemented at the edge layer. At the same time, the bottom-up reduction in the number of required samples enabled by SDS leads to considerable power savings.

Furthermore, a Machine Learning (ML) algorithm such as reinforcement learning, Naïve Bayesian, or Support Vector Machine (SVM) can be added to the system to learn the behavior of the system and reach at the optimal configuration at the runtime. Although, such ML-based approaches require more computational resources, they are likely within the capacity of the resources currently available on many edge devices and on almost all edge gateways. Thus, the added level of self-

**TABLE II:** Performance summary and comparison with the state-of-the-art works.

Signal Type	ECG						Other IoT Signals		
Reference	[58]	[59]	[20]	[19]	[46]	This Work	[20]	[60]	This Work
Technique/Architecture	LLDC	CS	DC	DC	Adaptive Rate	SDS	DC	ADCS	SDS
Programmable Accuracy	Yes	Yes	Yes	No	Yes	Yes	Yes	Yes	Yes
Connectivity	NA	NA	BLE	BTv1.1	2.4GHz TRx	BLE	BLE	WiFi	BLE
CF	1 to 7.94	8 to 17	2.1 to 7.8	2.38	1 to 7.3	1 to 29	NA	1-2.8	1 to 25
System Power Saving	50 to 87%	NA	43 to 82%	43%	0 to 80%	45 to 90%	47 to 82%	0 to 50%	45 to 94%

awareness and autonomy of the system substantially increases and the system will become -to some extent- personalized too. The ML-based approach could also offload the designer from benchmarking applications at the design time, which in turn reduces the time-to-market.

### VIII. COMPARISON

Table II presents a performance summary of the proposed system and compares it with other state-of-the-art designs. The first part of the table focuses on comparing the proposed approach with the state-of-the art designs in the context of ECG monitoring applications. In the second part of the table, we have compared the proposed approach with other IoT applications. We have also analyzed and compared our own method when used in the above-mentioned two contexts.

In the context of ECG applications, we have compared our work with the following methods: lossless and lossy direct compression (LLDC), compressed sensing (CS), digital compression (DC), adaptive sampling rate, and Adaptive Data Compression Scheme (ADCS). As can be seen from Table II, SDS provides the highest power saving for the overall system. It also offers the largest range of CF. That is, up to  $1.7\times$  larger CF compared to the best work listed in the table, namely [59], and approximately  $3.7\times$  compared to others ([58], [20], and [46]). A larger CF means more flexibility for any system, especially self-aware systems, that is, by using the proposed SDS systems can adjust their sampling configuration and consequently their performance. Such a high flexibility is particularly valuable when the proposed method is used in new contexts and applications, where optimum performance should be learned online. In the context of other IoT applications, we can see that the proposed method outperforms [20] and [60]. In comparison to [60], the proposed method provides approximately  $2\times$  better power saving and  $9\times$  better CF. [20] does not report any value for the CF for non-ECG applications. Hence, we cannot compare our work with them in terms of CF, however, we can see that our proposed method can lead to  $\sim 1.15\times$  or more power saving.

Comparison of the performance of the proposed method in the context of the ECG application and other IoT signals also leads to another interesting observation. Namely, we can see that even though the proposed approach achieves a higher CF in ECG applications (compared to the general IoT applications), the maximum power saving achieved in ECG applications is slightly lower. This can be attributed to the fact that the ECG signal is typically more complex, with more frequent and sharper changes, as compared to typical IoT applications, for example, monitoring of the green-house environmental parameters. Thus, one would expect a lower CF. However, we need to bear in mind that due to the

slower changes in the typical IoT signals (e.g., environment temperature or humidity), the achievable CF most of the time is limited by  $N$ , whereas in the context of faster changing signals, such as ECG,  $\varepsilon \times T_S$  appears to be a more determining factor for the maximum achievable CF. This can be explained by the fact that the Nyquist rate of signals with occasional changes is determined by those occasional changes, even though they may happen very rarely. Hence, Nyquist rate is a significantly more conservative estimate for those signals than it is for signals with frequent and rapid changes, such as ECG. Nonetheless, the proposed approach can lead to a better overall power saving in the IoT applications (e.g., green-house monitoring), since despite a lower CF, the overall number of data transmissions (connection events) that are avoided thanks to the proposed method is higher. Note that as mentioned earlier, reducing the number of connection events, will save energy in both data transmission and Digital/RF setup process.

### IX. CONCLUSION

In this paper, we proposed using the SDS technique for processing data in a self-aware fashion on resource-constrained IoT cyber-physical and embedded systems. We have shown that this approach requires no hardware changes in the system. We have showcased the advantages of the proposed system for a wearable ECG patch used for bio-signal monitoring and disease detection, and a green-house monitoring system used to regulate the environmental conditions, namely, temperature and humidity, of a green-house. The advantages of using the SDS approach in improving the power consumption of the overall system are presented. We have also discussed the dependency of the power consumption to the sampling rate and system configurations. We have shown that using suitable configuration, significant power savings can be achieved at negligible to no cost to the performance of the system. We have discussed how the user can take advantage of the programmability of the sampling technique based on the application and have the reconstructed signal quality at the level that is needed to satisfy the requirements of the application at hand, while saving on the overall power consumption of the IoT system. We have also shown that such a self-aware system comes at -virtually- no costs to the system regarding the overheads of memory and processing time. Examples provided show that by using the signal-dependent sampling in ECG systems one can save up to 78% in power without causing any considerable adverse effects on the quality of the reconstructed signal. This saving was up to 94% in the case of temperature and humidity monitoring of a green-house. We advocate that signal-dependent sampling can produce similar advantages in many other CPSs and ESs, especially in those used for IoT applications.

## REFERENCES

- [1] D. Evans, "The internet of things, how the next evolution of the internet is changing everything," Cisco Internet Business Solutions Group (IBSG), White Paper, April 2011. [Online]. Available: [https://www.cisco.com/c/dam/en\\_us/about/ac79/docs/innov/IoT\\_IBSG\\_0411FINAL.pdf](https://www.cisco.com/c/dam/en_us/about/ac79/docs/innov/IoT_IBSG_0411FINAL.pdf)
- [2] "Cisco annual internet report (2018–2023)," Cisco Internet Business Solutions Group (IBSG), White Paper, March 2020. [Online]. Available: <https://www.cisco.com/c/en/us/solutions/collateral/executive-perspectives/annual-internet-report/white-paper-c11-741490.pdf>
- [3] D. Xue and W. Huang, "Smart agriculture wireless sensor routing protocol and node location algorithm based on internet of things technology," *IEEE Sensors Journal*, pp. 1–1, 2020.
- [4] ———, "Smart agriculture wireless sensor routing protocol and node location algorithm based on internet of things technology," *IEEE Sensors Journal*, pp. 1–1, 2020.
- [5] S. K. S. Tyagi, A. Mukherjee, S. R. Pokhrel, and K. K. Hiran, "An intelligent and optimal resource allocation approach in sensor networks for smart agri-iot," *IEEE Sensors Journal*, pp. 1–1, 2020.
- [6] T. Liang and Y. J. Yuan, "Wearable medical monitoring systems based on wireless networks: A review," *IEEE Sensors Journal*, vol. 16, no. 23, pp. 8186–8199, 2016.
- [7] X. Bian, W. Xu, Y. Wang, L. Lu, and S. Wang, "Direct feature extraction and diagnosis of ecg signal in the compressed domain," *IEEE Sensors Journal*, pp. 1–1, 2021.
- [8] N. TaheriNejad, "Wearable medical devices: Challenges and self-aware solutions," in *IEEE Life Sciences*, vol. 2, April 2019, pp. 5–6.
- [9] K.-D. Kim and P. Kumar, "An overview and some challenges in cyber-physical systems," *Journal of the Indian Institute of Science*, vol. 93, no. 3, pp. 341–352, 2013.
- [10] S. Mittal, "A survey of techniques for improving energy efficiency in embedded computing systems," *arXiv preprint arXiv:1401.0765*, 2014.
- [11] L. Wang and Y. Xiao, "Energy saving mechanisms in sensor networks," in *2nd International Conference on Broadband Networks*, 2005., Oct 2005, pp. 724–732 Vol. 1.
- [12] V. Tenentes, D. Rossi, and B. M. Al-Hashimi, "Collective-aware system-on-chips for dependable iot applications," in *2018 IEEE 24th International Symposium on On-Line Testing And Robust System Design (IOLTS)*, July 2018, pp. 57–60.
- [13] A. Anzaniour *et al.*, "Self-awareness in remote health monitoring systems using wearable electronics," in *Design and Test Europe Conference (DATE)*, 2017. [Online]. Available: <http://jantsch.se/AxelJantsch/papers/2017/ArmanAnzaniour-DATE.pdf>
- [14] N. TaheriNejad, M. A. Shami, and S. M. P. D., "Self-aware sensing and attention-based data collection in multi-processor system-on-chips," in *2017 15th IEEE International New Circuits and Systems Conference (NEWCAS)*, June 2017, pp. 81–84.
- [15] P. Wei and F. He, "The compressed sensing of wireless sensor networks based on internet of things," *IEEE Sensors Journal*, pp. 1–1, 2021.
- [16] D. L. Donoho, "Compressed sensing," *IEEE Transactions on Information Theory*, vol. 52, no. 4, pp. 1289–1306, April 2006.
- [17] E. J. Candes and M. B. Wakin, "An introduction to compressive sampling," *IEEE Signal Processing Magazine*, vol. 25, no. 2, pp. 21–30, March 2008.
- [18] H. M. Al-Kadhim and H. S. Al-Raweshidy, "Energy efficient data compression in cloud based iot," *IEEE Sensors Journal*, vol. 21, no. 10, pp. 12 212–12 219, 2021.
- [19] E. Chua and W. Fang, "Mixed bio-signal lossless data compressor for portable brain-heart monitoring systems," *IEEE Transactions on Consumer Electronics*, vol. 57, no. 1, pp. 267–273, 2011.
- [20] C. J. Deepu, C.-H. Heng, and Y. Lian, "A hybrid data compression scheme for power reduction in wireless sensors for iot," *IEEE Transactions on Biomedical Circuits and Systems*, vol. 11, no. 2, pp. 245–254, 2017.
- [21] F. A. Marvasti, *Nonuniform Sampling : Theory and Practice*. Kluwer academic/Plenum, 2001.
- [22] Y. Tsividis, "Event-driven data acquisition and continuous-time digital signal processing," in *IEEE Custom Integrated Circuits Conference 2010*, Sep. 2010, pp. 1–8.
- [23] E. H. Hafshejani, M. Elmí, N. TaheriNejad, A. Fotowat-Ahmady, and S. Mirabbasi, "A low-power signal-dependent sampling technique: Analysis, implementation, and applications," *IEEE Transactions on Circuits and Systems I: Regular Papers*, pp. 1–14, 2020.
- [24] Y. Li, Y. Sun, G. Dai, Y. Wang, J. Ni, Y. Wang, G. Li, and H. Yang, "A self-aware data compression system on FPGA in hadoop," in *2015 International Conference on Field Programmable Technology (FPT)*, 2015, pp. 196–199.
- [25] J.-S. Preden, K. Tammemäe, A. Jantsch, M. Leier, A. Riid, and E. Calis, "The benefits of self-awareness and attention in fog and mist computing," *IEEE Computer, Special Issue on Self-Aware/Expressive Computing Systems*, pp. 37–45, July 2015.
- [26] A. Jantsch, N. Dutt, and A. M. Rahmani, "Self-awareness in systems on chip – a survey," *IEEE Design Test*, vol. 34, no. 6, pp. 1–19, December 2017. [Online]. Available: <http://jantsch.se/AxelJantsch/papers/2017/AxelJantsch-DesignTest.pdf>
- [27] K. Tammemäe, A. Jantsch, A. Kuusik, J.-S. Preden, and E. Öunapuu, *Self-Aware Fog Computing in Private and Secure Spheres*. Cham: Springer International Publishing, 2018, pp. 71–99.
- [28] K. Bellman, N. Dutt, L. Esterle, A. Herkersdorf, A. Jantsch, C. Landauer, P. R. Lewis, M. Platzner, N. TaheriNejad, and K. Tammemäe, "Self-aware cyber-physical systems," *ACM Transactions on Cyber-Physical Systems*, pp. 1–24, 2020.
- [29] H. A. Khaderi *et al.*, "Enhancement of classification of small data sets using self-awareness; an iris flower case-study," in *2018 IEEE International Symposium on Circuits and Systems (ISCAS)*, May 2018, pp. 1–5.
- [30] F. Forooghifar *et al.*, "Self-aware wearable systems in epileptic seizure detection," in *Euromicro Conference on Digital System Design (DSD)*, 2018.
- [31] K. Neshatpour *et al.*, "ICNN: An iterative implementation of convolutional neural networks to enable energy and computational complexity aware dynamic approximation," in *2018 Design, Automation Test in Europe Conference Exhibition (DATE)*, March 2018, pp. 551–556.
- [32] A. Mozelli, N. TaheriNejad, and A. Jantsch, "A study on confidence: an unsupervised multi-agent machine learning experiment," *IEEE Design Test*, pp. 1–1, 2021.
- [33] M. Götzinger, N. TaheriNejad, H. A. Khaderi, and A. Jantsch, "On the design of context-aware health monitoring without a priori knowledge; an AC-motor case-study," in *2017 IEEE 30th Canadian Conference on Electrical and Computer Engineering (CCECE)*. IEEE, 2017, pp. 1–5.
- [34] M. Goetzinger *et al.*, "Applicability of context-aware health monitoring to hydraulic circuits," in *IECON 2018 - 44th Annual Conference of the IEEE Industrial Electronics Society*, Oct 2018, pp. 4712–4719.
- [35] M. Götzinger *et al.*, "Enhancing the self-aware early warning score system through fuzzified data reliability assessment," in *International Conference on Wireless Mobile Communication and Healthcare*. Springer, 2017.
- [36] N. Dutt and N. TaheriNejad, "Self-awareness in cyber-physical systems," in *2016 29th International Conference on VLSI Design and 2016 15th International Conference on Embedded Systems (VLSID)*, Jan 2016, pp. 5–6.
- [37] D. B. Abeywickrama and E. Ovaska, "A survey of autonomic computing methods in digital service ecosystems," *SOCA*, vol. 11, p. 1–31, 2017.
- [38] S. Sarma, N. Dutt, P. Gupta, A. Nicolau, and N. Venkatasubramanian, "On-chip self-awareness using cyberphysical-systems-on-chip (cpsoc)," in *2014 International Conference on Hardware/Software Codesign and System Synthesis (CODES+ISSS)*, Oct 2014, pp. 1–3.
- [39] F. D. Macías-Escrivá, R. Haber, R. del Toro, and V. Hernandez, "Self-adaptive systems: A survey of current approaches, research challenges and applications," *Expert Systems with Applications*, vol. 40, no. 18, pp. 7267–7279, 2013. [Online]. Available: <https://www.sciencedirect.com/science/article/pii/S0957417413005125>
- [40] TI, "CC2650, SimpleLink Multistandard Wireless MCU," Texas Instruments (TI), Data Sheet, July 2016. [Online]. Available: <http://www.ti.com/lit/ds/symlink/cc2650.pdf>
- [41] Bluetooth, "Bluetooth Specification Version 4.2," Bluetooth, Tech. Rep., December 2014. [Online]. Available: <https://www.bluetooth.com/specifications>
- [42] ———, "Bluetooth smart or version 4.0+ of the bluetooth specification," Bluetooth Organization, Technical Reference, 2010. [Online]. Available: <https://www.bluetooth.com>
- [43] K. Townsend, R. Davidson, and C. Cufí, *Getting Started with Bluetooth Low Energy*. O'Reilly, 2014. [Online]. Available: <https://books.google.ca/books?id=XjY4nwEACAAJ>
- [44] e. a. Joakim Lindh, "Measuring bluetooth low energy power consumption," Texas Instruments (TI), Application Note, January 2019. [Online]. Available: <http://www.ti.com/lit/an/swra478d/swra478d.pdf>
- [45] D. Griffith, J. Murdock, and P. T. Roine, "5.9 a 24mhz crystal oscillator with robust fast start-up using dithered injection," in *2016 IEEE*

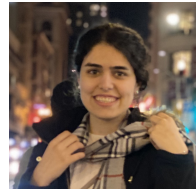
- International Solid-State Circuits Conference (ISSCC)*, Jan 2016, pp. 104–105.
- [46] R. F. Yazicioglu *et al.*, “A 30 $\mu$ w analog signal processor asic for portable biopotential signal monitoring,” *IEEE Journal of Solid-State Circuits*, vol. 46, no. 1, pp. 209–223, Jan 2011.
- [47] F. Chen, A. P. Chandrakasan, and V. Stojanović, “A signal-agnostic compressed sensing acquisition system for wireless and implantable sensors,” in *IEEE Custom Integrated Circuits Conference 2010*, Sep. 2010, pp. 1–4.
- [48] C. Weltin-Wu and Y. Tsividis, “An event-driven clockless level-crossing adc with signal-dependent adaptive resolution,” *IEEE Journal of Solid-State Circuits*, vol. 48, no. 9, pp. 2180–2190, Sep. 2013.
- [49] ST, “ARM Cortex-M4 32b MCU+FPU,” ST Microelectronics (ST), Data Sheet, September 2016. [Online]. Available: <https://www.st.com/resource/en/datasheet/dm00037051.pdf>
- [50] e. a. Goldberger AL, “Physiobank, physiotoolkit, and physionet: Components of a new research resource for complex physiologic signals. circulation 101(23):e215-e220 [circulation electronic pages; http://circ.ahajournals.org/content/101/23/e215.full]; 2000 (june 13); MIT, Tech. Rep., June 2000. [Online]. Available: <http://circ.ahajournals.org/content/101/23/e215.full>
- [51] T. Regan *et al.*, “Current sense circuit collection,” Analog Devices (AD), Application Note, December 2005. [Online]. Available: <https://www.analog.com/media/en/technical-documentation/application-notes/an105fa.pdf>
- [52] U. R. Acharya, *Advances in Cardiac Signal Processing*. Springer Science & Business Media, 2007.
- [53] E. Ataman, V. Aatre, and K. Wong, “A fast method for real-time median filtering,” *IEEE Transactions on Acoustics, Speech, and Signal Processing*, vol. 28, no. 4, pp. 415–421, August 1980.
- [54] J. H. O’Keefe *et al.*, *The Complete Guide to ECGs: A Comprehensive Study Guide to Improve ECG Interpretation Skills*, 5th ed. Jones and Bartlett Learning, 2010.
- [55] R. P. Jaakkola Malmivuo, *Bioelectromagnetism: Principles and Applications of Bioelectric and Biomagnetic Fields*. OXFORD UNIVERSITY PRESS, 1995.
- [56] B. Surawicz and T. Knilans, *Chou’s Electrocardiography in Clinical Practice*, 6th ed. Saunders, 2008.
- [57] A. L. Goldberger, *Clinical Electrocardiography: A Simplified Approach*. The Mosby Company, 1977.
- [58] S. Lin, H. Lin, and Y. Lin, “Lossless and lossy direct compression design with multi-signal symptom detection for low-temperature wearable devices,” *IEEE Sensors Journal*, vol. 19, no. 2, pp. 715–725, 2019.
- [59] Y. Wang, X. Li, K. Xu, F. Ren, and H. Yu, “Data-driven sampling matrix boolean optimization for energy-efficient biomedical signal acquisition by compressive sensing,” *IEEE Transactions on Biomedical Circuits and Systems*, vol. 11, no. 2, pp. 255–266, 2017.
- [60] H. M. Al-Kadhim and H. S. Al-Raweshidy, “Energy efficient data compression in cloud based iot,” *IEEE Sensors Journal*, vol. 21, no. 10, pp. 12 212–12 219, 2021.



**Ehsan Hadizadeh** received a B.S. degree in Electrical Engineering from Shahrekhord University in 2010 and a M.S. degree from Sharif University of Technology in 2013. He is currently a Ph.D. student at Sharif University of Technology and a visiting research scholar at the Electrical and Computer Engineering department of the University of British Columbia. His research interests include RF/Analog IC design and ultra-low power systems.



**Nima TaheriNejad** (S’08-M’15) received his Ph.D. degree in electrical and computer engineering from The University of British Columbia (UBC), Vancouver, Canada, in 2015. He is currently an assistant professor at the TU Wien (formerly known as Vienna University of Technology as well), Vienna, Austria, where his areas of work include self-awareness in resource-constrained cyber-physical (embedded) systems, systems on chip, health-care, computer architecture, in-memory computing, and memristor-based circuit and systems.



**Rozhan Rabbani** received a B.S. degree in Electrical Engineering from Sharif University of Technology, Tehran, Iran, in 2018. Her B.S. research was focused on Analog/Mixed signal IC design, RF circuits and biomedical systems. She is currently a Ph.D. student at the Electrical Engineering and Computer Science department at University of California, Berkeley. Her research interests are biomedical circuits and sensor design and low-power implants.



**Zohreh Azizi** received a B.S. degree in Electrical Engineering from Sharif University of Technology, Tehran, Iran, in 2018. Her B.S. background is in circuit design, MEMS, and biomedical electronics. She is currently a Ph.D. student at the Electrical and Computer Engineering department of the University of Southern California, Los Angeles, CA, USA. Currently, her research is focused on image processing, machine learning, and computer vision.



**Shahabeddin Mohin** received the B.Sc. and M.Sc. degrees in electrical engineering from Sharif University of Technology, Tehran, Iran, in 2018 and 2020, respectively. He is currently working toward the Ph.D. degree with the Department of Electrical Engineering and Computer Science, Massachusetts Institute of Technology (MIT), Cambridge, MA. His current research interests include RF and mm-Wave integrated circuits for wireless applications. He was a recipient of the Gold Medal winner of the National Astronomy Olympiad in Iran, in 2013, the Gold Medal winner of the International Olympiad on Astronomy and Astrophysics (IOAA) in Romania, in 2014, and the best data analysis Award in IOAA 2014.



**Ali Fotowat-Ahmady** (M’80) was born in Tehran, Iran, in 1958. He received the B.S. degree from California Institute of Technology, Pasadena, CA, USA, in 1980, and the M.S. and Ph.D. degrees in electrical engineering from Stanford University, Stanford, CA, USA, in 1982 and 1991, respectively. He started his career at Philips Semiconductor in Sunnyvale, CA, USA, in 1987 where he developed several integrated circuits for mobile phones. Since 1992, he has been with the Department of Electrical Engineering at Sharif University of Technology, Iran, where he is an Associate Professor.



**Shahriar Mirabbasi** (S’95-M’02) received the B.Sc. degree in electrical engineering from Sharif University of Technology, Tehran, Iran, in 1990, and the M.A.Sc. and Ph.D. degrees in electrical and computer engineering from the University of Toronto, Toronto, ON, Canada, in 1997 and 2002, respectively. Since August 2002, he has been with the Department of Electrical and Computer Engineering, University of British Columbia, Vancouver, BC, Canada where he is currently a Professor. His current research interests include analog, mixed-signal, RF, and mm-wave integrated circuit and system design with an emphasis on communication, sensor interface, and biomedical applications.